Increase of ferromagnetic ordering temperature by the minority-band double-exchange interaction in $SrRu_{1-x}Cr_xO_3$

B. Dabrowski, S. Kolesnik, O. Chmaissem, and T. Maxwell
Physics Department, Northern Illinois University, DeKalb, Illinois 60115, USA

M. Avdeev, P. W. Barnes, and J. D. Jorgensen
Materials Science Division, Argonne National Laboratory, Argonne, Illinois 60439, USA
(Received 20 May 2005; published 19 August 2005)

Structural, magnetic, and resistive properties of the chromium substituted $SrRu_{1-x}Cr_xO_3$ perovskites with increased ferromagnetic transition temperature from 163 to 188 K were studied for polycrystalline samples synthesized in air and at high pressure. The Cr solubility limit found at $x=0.15$ in air is controlled by geometrical constraints of the tolerance factor and can be extended to higher values through high-pressure synthesis at 3 GPa. A linear decrease of the lattice parameters and bond lengths and an increase of the bond angles with x are consistent with the substitution of smaller $Cr^{4+/3+}$ for $Ru^{4+/5+}$. Similar decreases of the magnetic susceptibility χ_m in the paramagnetic region above T_c and the high-field magnetization at 5 K with increasing x also indicate the presence of the $Cr^{4+/3+}$ and $Ru^{4+/5+}$ ions. This chemical substitution creates a possible $Ru^{4+/5+}(d^{4/3})$-O^{2-}-$Cr^{4+/3+}(d^{2/3})$ minority band double-exchange interaction which involves the Cr^{3+} and Cr^{4+} in magnetic ordering that enhances the ordering temperature. A reduced coercive field determined from the magnetization curves and a minimum of the resistivity point to decreased disorder for slightly substituted compositions $x\sim 0.025$.

DOI: 10.1103/PhysRevB.72.054428 PACS number(s): 75.50.Dd, 61.66.Fn, 61.12.−q, 75.30.Cr

I. INTRODUCTION

Ferromagnetic 4*d* perovskite $SrRuO_3$ has recently attracted increased attention due to its rich electronic and magnetic properties arising from ferromagnetic alignment of the low-spin t_g^4 electrons of Ru^{4+} (Refs. 1 and 2) and possible technological application as an electrode material in microelectronic circuits.[3] Stoichiometric $SrRuO_3$ orders ferromagnetically below $T_c=163$ K and at 300 kOe has an ordered moment of 1.6 μ_B/Ru, far short of the expected full $S=1$ moment (2 μ_B/Ru atom).[4] Reduced moment and the metallic conductivity are consistent with itinerant ferromagnetism.[2,5] Recently, we have shown that annealing of $SrRuO_3$ in high-pressure oxygen produces $SrRu_{1-v}O_3$ compounds with randomly distributed vacancies on the Ru site.[6] The creation of Ru vacancies rapidly suppresses the T_c to 45 K with an increase of v to 0.09 and decreases the ordered moment to $\sim$0.8 μ_B/Ru.[6,7] Reduced Curie temperatures have been also observed for thin films deposited on substrates with mismatched lattice parameters,[8] single crystals that were grown in alumina crucibles,[4] and chemically substituted $SrRuO_3$ compounds.[9,10] Substitution of isovalent Ca for Sr suppresses ferromagnetism while maintaining the metallic conductivity. This was explained by an increased orthorhombic distortion and a larger deviation of the Ru-O-Ru bond angle from 180°.[2,4,11] A small concentration of Na reduces T_c rapidly and induces an insulating state[12] similar to Zn^{2+}, Ni^{2+}, Co^{2+}, and Mn^{3+} substitutions into the Ru site.[13] These suppressed T_c's are thought to be due to the change in Ru formal oxidation state and destructive interaction between the electronic orbitals of the substituted cations with the Ru t_{2g} band, which results in a narrowed bandwidth.[13]

The lone exception found to increase T_c is the substitution of Cr on the Ru site. T_c reaches a value of 188 K when 10% Cr is substituted onto the Ru site.[13] A broadened Ru t_{2g} bandwidth is the suspected origin of this effect.[13] We have recently initiated study of this unique $SrRu_{1-x}Cr_xO_3$ system and performed local studies of Ru and Cr valence state using nuclear magnetic resonance spectroscopy (NMR) and magnetization measurements for two Cr-substituted samples with $x=0.05$ and 0.12.[14] These studies show a valence state of Cr^{3+} and an average valence of $Ru^{(4+\delta)+}$, which indicate that the spin-down electron in the Ru 4*d* band is less localized. This creates the possibility of a $Ru^{4+/5+}(d^{4/3})$-O^{2-}-$Cr^{4+/3+}(d^{2/3})$ minority band double-exchange interaction which involves the Cr^{3+} and Cr^{4+} in the magnetic ordering and enhances the ordering temperature. In the present paper we describe in detail the synthesis and structural, magnetic, and resistive properties of homogenous $SrRu_{1-x}Cr_xO_3$ ($x=0-0.2$) samples stabilized in the perovskite phase by the random substitution of Cr for Ru. Dependence of structural parameters of bond lengths and the properties of magnetic susceptibility χ_m in the paramagnetic region show presence of Cr^{4+} ion in magnetic interactions, thus providing additional evidence for the double-exchange enhancement of T_c.

II. SYNTHESIS AND EXPERIMENTAL PROCEDURES

Polycrystalline samples of stoichiometric $SrRuO_3$ and Cr-substituted $SrRu_{1-x}Cr_xO_3$ compounds with $x=0.01$, 0.025, 0.05, 0.075, 0.10, 0.125, 0.15, and 0.20 were synthesized from mixtures of $SrCO_3$, RuO_2 (prefired in air at 600 °C), and Cr_2O_3. Calcination of the starting mixtures was done for short periods of time at 800 °C to avoid the conspicuous volatility of RuO_2 at elevated temperatures. The intimately

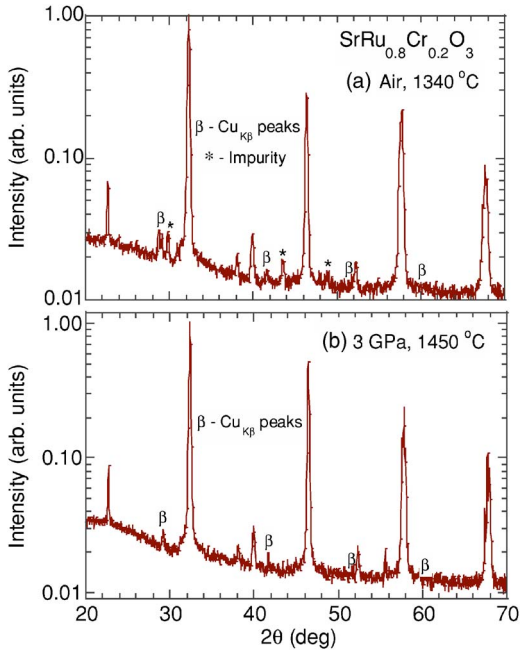

FIG. 1. (Color online) X-ray diffraction patterns for the $SrRu_{0.8}Cr_{0.2}O_3$ sample prepared in air at 1340 °C (a) and in 3 GPa at 1450 °C (b). Diffraction peaks corresponding to impurity phase are denoted with asterisks. The small reflections at 28.7, 41.7, 51.6, and 60.2 are diffraction peaks corresponding to the $Cu_{K\beta}$ radiation of the highest intensity Bragg peaks.

mixed powders were then pressed into pellets and fired in air at increasing temperatures with several intermediate grindings up to the final sintering temperature of 1100 and 1340 °C for $x=0$ and $x\neq 0$ samples, respectively. The 2 g samples were obtained and examined by x-ray diffraction at room temperature on a Rigaku D/MAX Diffractometer using $Cu_{K\alpha}$ radiation. Within the sensitivity limit ($\approx 3\%$), the air synthesized samples with $x<0.15$ are single phase with the $GdFeO_3$-like orthorhombic structure. Samples with $x\geqslant 0.15$ showed small amounts of impurity phases that could not be removed by changing the synthesis temperature or oxygen pressure at normal conditions. We have found, however, that preparation of materials with Cr substitution levels greater than 0.15 can be accomplished through high-temperature high-pressure synthetic methods. The high-pressure high-temperature reaction was carried out on a prefired mixture with a stoichiometry equivalent to $SrRu_{0.8}Cr_{0.2}O_3$. High pressure (3 GPa) was applied using a cubic single-stage multianvil apparatus. The sample was pressed into small pellets (diameter=0.1811 in.), placed in a small alumina capsule, pressurized to 3 GPa, and heated to 1450 °C for 2 h before quenching. Complete details for the cubic anvil high-pressure apparatus, pressure cell assembly, temperature and pressure calibrations will be described in a future publication. Figure 1 shows exemplary x-ray diffraction patterns for the $x=0.2$ sample prepared under normal and high-temperature high-pressure conditions. The data are plotted on a logarithmic scale to better depict the small amounts of impurity phases observed for the sample prepared under normal conditions.

ac susceptibility and static (dc) magnetization were carried out on a Magnetic Property Measurement System (MPMS, Quantum Design). The resistive properties of the samples were determined from standard 4-point measurements performed on rectangular bars cut from pressed pellets using a Physical Property Measurement System 6000 (PPMS, Quantum Design) for 5 K$<T<$400 K.

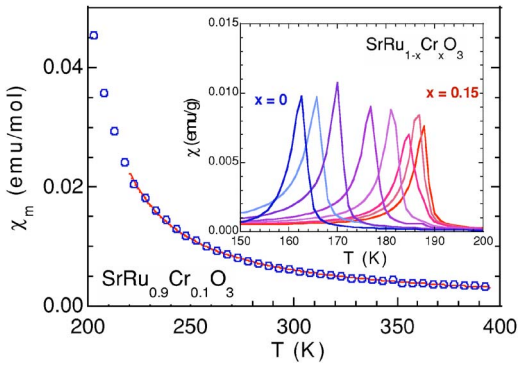

FIG. 2. (Color online) Temperature dependence of the magnetic susceptibility for $SrRu_{0.9}Cr_{0.1}O_3$ in the paramagnetic region. The solid line is a fit of a Curie Weiss formula to the data. The inset shows ac susceptibility data near the ferromagnetic transition temperature for single-phase samples of $SrRu_{1-x}Cr_xO_3$ obtained from synthesis in air.

Time-of-flight neutron powder diffraction data for the single-phase $Sr(Ru_{1-x}Cr_x)O_3$ samples were collected at room temperature on the Special Environment Powder Diffractometer[15] (SEPD) at the Intense Pulsed Neutron Source (IPNS) at Argonne National Laboratory. High-resolution backscattering data (detector bank 1, $2\theta=144.85°$) were analyzed using the Rietveld method with the GSAS (EXPGUI) suite.[16,17]

III. RESULTS AND DISCUSSION

A. Magnetic and resistive properties

Temperature dependencies of the ac susceptibility near the ferromagnetic transition are presented in the inset to Fig. 2 for single-phase samples of $SrRu_{1-x}Cr_xO_3$ obtained from synthesis in air. All samples exhibit very sharp transitions that could be achieved only after several firings at high temperatures.[4] The Curie temperatures, T_c, determined from maximums of the peaks in ac susceptibility curves, initially show a rapid increase with increasing Cr substitution saturating around $x=0.15$. The T_c of $SrRu_{0.8}Cr_{0.2}O_3$ that was synthesized at ambient pressure is the same as that observed for the $x=0.15$ sample, clearly in agreement with the x-ray diffraction and the phase rule that suggests the solubility limit of chromium substitution is around $x=0.15$. Temperature dependence of the ac susceptibility for the high pressure $SrRu_{0.8}Cr_{0.2}O_3$ sample shows a clear decrease in T_c by 13 K. Thus, substitution of a larger amount of Cr for Ru, achieved only by high-pressure synthesis when $x>0.15$, rapidly suppresses T_c.

The magnetic susceptibility, χ_m, in the temperature range 220–400 K (in the paramagnetic region above T_c, plotted in Fig. 2 for $x=0.1$) was used to determine the effective paramagnetic moment μ_{eff}, by fitting the Curie-Weiss formula

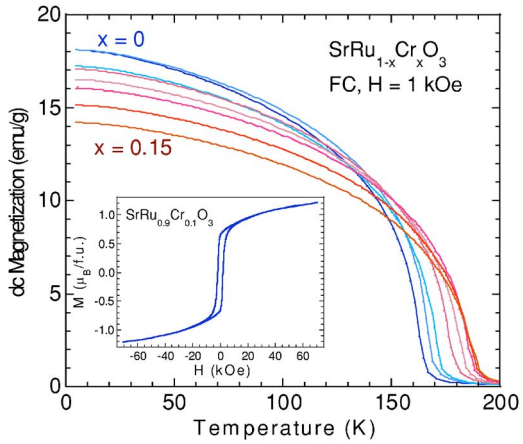

FIG. 3. (Color online) Temperature dependence of the magnetization for single-phase samples of $SrRu_{1-x}Cr_xO_3$ obtained from synthesis in air. The inset shows the magnetization hysteresis curve measured at 5 K for $SrRu_{0.9}Cr_{0.1}O_3$.

$\chi_m = \chi_0 + (1/8)\mu_{\text{eff}}^2/(T-\Theta)$. In this formula χ_0 is a constant susceptibility and Θ is the paramagnetic Curie temperature. Temperature dependence of the dc magnetization shown in Fig. 3 clearly exhibits a behavior characteristic of high quality ferromagnetic materials with a steep increase below T_c. Magnetization hysteresis curves, shown in the inset to Fig. 3 for $SrRu_{0.9}Cr_{0.1}O_3$, does not saturate in magnetic fields up to 70 kOe, similar to pure $SrRuO_3$. The characteristic parameters determined from the magnetization curves, namely the high-field magnetization M (5 K), coercivity field H_{coer}, and remnant magnetization M_{rem}, as well as T_c's and μ_{eff} determined from the ac susceptibility are listed in Table I for all single-phase samples.

With increasing Cr substitution the high-field magnetization M (5 K) gradually decreases indicating effective antiferromagnetic coupling of the Ru and Cr ions (Table I). This coupling could involve a double-exchange interaction that enhances T_c between the minority Ru t_{2g} band and the Cr t_{2g} band. From the low-temperature magnetization measurements alone it is not possible to provide definitive evidence for the presence of the Cr^{4+} ion in these interactions since various Ru and Cr valence and electronic configurations estimate the same reduction of magnetization $M(5\text{ K}) = (2-4x)\mu_B$ for both $Sr(Ru^{4+(\uparrow\uparrow\uparrow\downarrow)}{}_{1-x}Cr^{4+(\downarrow\downarrow)}{}_x)O_3$ and $Sr(Ru^{5+(\uparrow\uparrow\uparrow)}{}_xRu^{4+(\uparrow\uparrow\uparrow\downarrow)}{}_{1-2x}Cr^{3+(\downarrow\downarrow\downarrow)}{}_x)O_3$ configurations. However, these two different combinations of oxidation states of $Ru^{4+/5+}$ and $Cr^{4+/3+}$ should give different values of the effective paramagnetic moment $\mu_{\text{eff}} = g\sqrt{S(S+1)}$ where $g=2$ is the Landé factor and S is the effective spin. Assuming the spin state of each cation of $S(Ru^{4+})=1$, $S(Ru^{5+})=3/2$, $S(Cr^{4+})=1$ and $S(Cr^{3+})=3/2$, the expected μ_{eff} for $Sr(Ru^{4+}{}_{1-x}Cr^{4+}{}_x)O_3$ is independent of x and equal to 2.83. For the charge balance state $Sr(Ru^{5+}{}_xRu^{4+}{}_{1-2x}Cr^{3+}{}_x)O_3$, the μ_{eff} should increase with x according to the formula $\mu_{\text{eff}}^2 = g^2[(1-2x)1(1+1)+(x+x)3/2(3/2+1)]$. The measured values of μ_{eff} shown in Fig. 4(a) demonstrate a slight decrease with increasing x. This behavior is closer to the expected charge balance of the $Sr(Ru^{4+}{}_{1-x}Cr^{4+}{}_x)O_3$ configuration; i.e.,

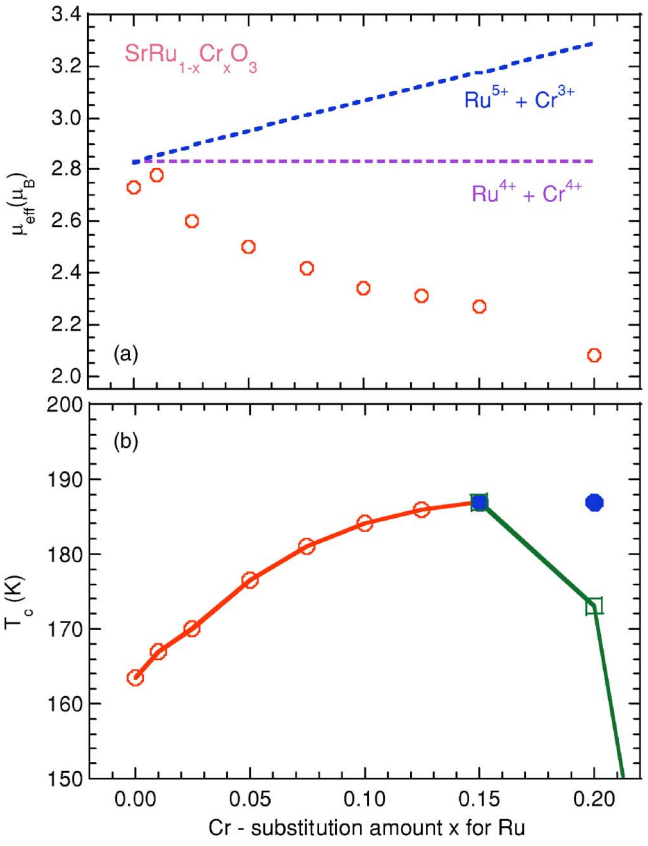

FIG. 4. (Color online) Compositional dependence of the effective paramagnetic moment μ_{eff} [broken lines depict expected dependence of the Ru and Cr charge states for $Sr(Ru^{4+}{}_{1-x}Cr^{4+}{}_x)O_3$ and $Sr(Ru^{5+}{}_xRu^{4+}{}_{1-2x}Cr^{3+}{}_x)O_3$] (a) and ferromagnetic transition temperatures for single-phase samples synthesized in air (open circles) and 3 GPa (open squares) and multiphase samples synthesized in air (filled circles) (b).

TABLE I. Magnetic and transport parameters for $SrRu_{1-x}Cr_xO_3$.

x	0	0.01	0.025	0.05	0.075	0.10	0.125	0.15	0.20
T_c (K)	163	167	170	177	181	185	187	188	177
M(70 kOe,5 K) (μ_B/f.u.)	1.44	1.46	1.35	1.32	1.25	1.21	1.16	1.21	0.92
H_{coer}(5 K) (kOe)	2.16	1.47	1.37	1.49	1.68	1.89	2.00	3.10	2.43
μ_{eff} (μ_B)	2.73	2.78	2.60	2.50	2.42	2.34	2.31	2.27	2.06
M_{rem} (μ_B/f.u.)	0.78	0.74	0.70	0.68	0.65	0.65	0.62	0.59	0.43
ρ(300 K) (mΩ cm)	1.50	1.09	1.19	1.45	2.23	3.20	2.17	7.73	

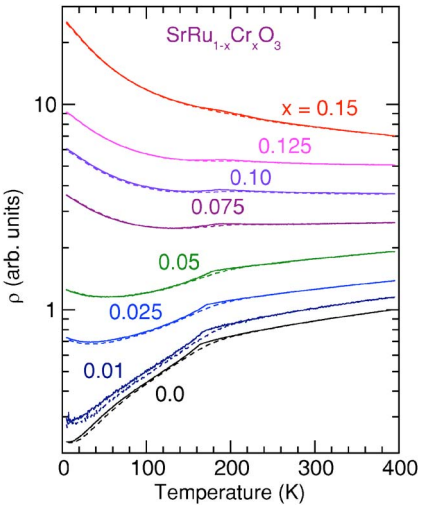

FIG. 5. (Color online) Normalized resistivity on a logarithmic scale for ceramic $SrRu_{1-x}Cr_xO_3$ samples. The measurements were taken in a zero magnetic field (solid lines) and in a magnetic field of 70 kOe (dashed lines). The data are shifted along the y axis for clarity.

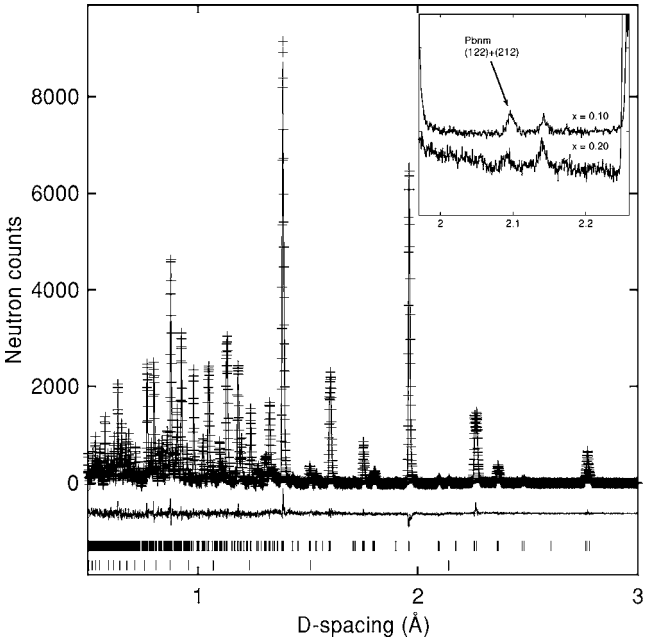

FIG. 6. Best-fit Rietveld refinement of TOF neutron powder diffraction data at RT for $SrRu_{0.9}Cr_{0.1}O_3$. Plus symbols are observed data from Bank 1 (2θ=144.85°), and continuous lines are the calculated profile and the difference curve. Upper and lower tick marks indicate the perovskite phase and vanadium of the sample can, respectively. The inset shows reflections allowed in *Pbnm* and forbidden in *Imma* for x=0.10 (upper curve) and x=0.20 (lower curve). For structural details, see Table II.

it indicates presence of the Cr^{4+} ion that could participate in double exchange interactions. It should be pointed out that assigning integer valences for Ru and Cr in an itinerant system is not strictly valid and is used here only as a useful approximation.

The coercive fields listed in Table I initially decrease, achieve a minimum at x=0.025, and increase for larger x. This behavior indicates decreased pinning of magnetic domain walls for slightly Cr substituted materials. It is intriguing to hypothesize that decreased pinning may arise from decreased disorder resulting from removal of a small amount of possible Ru vacancies in $SrRuO_3$.[6] This would indicate that a simple method of chemical substitution could prevent formation of Ru vacancies and simultaneously enhance electronic and magnetic properties of $SrRuO_3$.

The normalized resistivity of ceramic $SrRu_{1-x}Cr_xO_3$ samples collected from 5 to 400 K is presented in Fig. 5. The resistivity is shown on a logarithmic scale to emphasize a gradual change from metallic to semiconducting behavior as a function of increasing Cr content x. Metallic behavior is observed above and below T_c for lightly Cr substituted samples $x \leqslant 0.05$. A further increase of the Cr content changes the character of the resistivity to semiconducting/insulating. All samples show a clear decrease of resistivity below the ferromagnetic transition temperature due to decreased magnetic scattering. This supports a model of the double exchange interactions and proves that Cr is actively involved in the magnetic interactions. The resistive transitions give values for T_c similar to those obtained from the magnetic measurements as shown in Fig. 4(b). In addition, a small negative magnetoresistance is present for all samples near T_c. The absolute magnitudes of resistivity at 300 K are listed in Table I. The lowest resistivity values at room temperature that are observed for the x=0.01 and 0.025 samples may indicate a broadened Ru t_{2g} bandwidth and less defect scattering in agreement with the NMR (Ref. 14) and coercivity field measurements. However, the scatter of measured resistivities indicates a considerable contribution of the grain boundary resistance of polycrystalline samples, thus, preventing unqualified conclusions.

B. Structural properties

Neutron powder diffraction data for all studied compositions $SrRu_{1-x}Cr_xO_3$, x=0–0.20 have been successfully refined in the orthorhombic *Pbnm* space group with agreement factors R_p, R_{wp}, and χ^2 of 3–4 %, 5–9 %, and 1.3–1.6, respectively. A plot of the best-fit Rietveld refinement of the time-of-flight neutron powder diffraction data at room temperature is illustrated in Fig. 6 for the x=0.10 sample. The x=0–0.125 samples are single phase and the x=0.15 composition located at the boundary of solubility limit shows traces of an unidentified impurity phase (lower tick marks in Fig. 6 indicate vanadium of the sample container). Structural results are summarized in Table II.

The evolution of the lattice parameters and unit cell volume with composition is presented in Figs. 7(a) and 7(b). The ionic radius of Cr^{3+} (0.615 Å) is very close to that of Ru^{4+} (0.62 Å).[18] Substitution for ruthenium might cause formation of smaller Ru^{5+} (0.565 Å) according to the charge balance $Sr(Ru^{5+}_{x}Ru^{4+}_{1-2x}Cr^{3+}_{x})O_3$ (Ref. 14) or formation of smaller Cr^{4+} (0.55 Å) according to the charge balance $Sr(Ru^{4+}_{1-x}Cr^{4+}_{x})O_3$. The average ionic radius of the B site would decrease in both cases causing a decrease of the cell parameters and cell volume. Thus, decrease of the average

TABLE II. Refined structural parameters for perovskite phases $SrRu_{1-x}Cr_xO_3$ at room temperature. Space group *Pbnm* (No. 62), with Sr at $4c(x,y,1/4)$, Ru/Cr at $4a(0,0,0)$, O1 at $8d(x,y,z)$, and O2 at $4c(x,y,1/4)$. Numbers in parentheses are statistical standard deviations of the last significant digit.

x	0 (Ref. 6)	0.01	0.025	0.05	0.075	0.10	0.125	0.15	0.20
a (Å)	5.57119(10)	5.56987(11)	5.56815(9)	5.56613(8)	5.56427(10)	5.56081(9)	5.55737(19)	5.55481(12)	5.54762(12)
b (Å)	5.53390(9)	5.53385(9)	5.53191(7)	5.53030(7)	5.52854(9)	5.52574(8)	5.52242(16)	5.52063(10)	5.51463(10)
c (Å)	7.8486(2)	7.8474(2)	7.8446(1)	7.8413(1)	7.8378(2)	7.8321(1)	7.8268(3)	7.8223(2)	7.8096(2)
v (Å^3)	241.977(4)	241.879(4)	241.632(4)	241.372(3)	241.108(4)	240.661(4)	240.204(7)	239.88(5)	238.918(5)
Ru/Cr–O1×2	1.9841(14)	1.9841(17)	1.9820(15)	1.9793(13)	1.9753(18)	1.9709(17)	1.9686(1)	1.9636(20)	1.964(4)
–O1×2	1.9865(15)	1.9861(17)	1.9845(15)	1.9837(13)	1.9834(18)	1.9823(17)	1.9819(1)	1.9806(20)	1.971(4)
–O2×2	1.9844(4)	1.9842(4)	1.9826(4)	1.9812(3)	1.9790(4)	1.9771(4)	1.9750(1)	1.9741(4)	1.9668(5)
Sr–O1×2	2.728(8)	2.728(3)	2.728(2)	2.725(2)	2.722(3)	2.720(3)	2.7201(1)	2.717(3)	2.709(5)
–O1×2	2.522(2)	2.520(3)	2.524(2)	2.530(2)	2.538(3)	2.544(3)	2.5453(1)	2.557(3)	2.566(5)
–O1×2	2.764(2)	2.767(2)	2.770(2)	2.771(2)	2.773(2)	2.780(3)	2.7767(1)	2.780(3)	2.797(4)
–O1×2	3.125(2)	3.121(2)	3.110(2)	3.098(2)	3.084(2)	3.064(2)	3.0578(1)	3.037(3)	2.999(5)
–O2	2.894(3)	2.891(3)	2.880(3)	2.877(3)	2.871(4)	2.856(4)	2.8506(1)	2.843(5)	2.814(12)
–O2	2.675(3)	2.677(3)	2.685(3)	2.686(3)	2.687(4)	2.699(4)	2.6987(1)	2.706(5)	2.722(12)
–O2	3.072(4)	3.073(4)	3.064(3)	3.062(3)	3.051(4)	3.045(4)	3.0434(1)	3.037(4)	3.004(6)
–O2	2.504(4)	2.501(4)	2.507(3)	2.508(3)	2.516(4)	2.518(4)	2.5161(1)	2.520(4)	2.544(6)
Ru/Cr-O1-Ru/Cr	162.85(8)	162.84(9)	163.31(8)	163.75(7)	164.38(10)	165.09(9)	165.42(8)	166.22(11)	166.90(18)
Ru/Cr-O2-Ru/Cr	162.81(15)	162.77(16)	163.14(14)	163.33(12)	163.88(16)	164.07(15)	164.12(13)	164.31(17)	165.20(28)

ionic radius of the B site reduces the structural distortion of the perovskite cell when the size of A site ion is fixed. This is observed as an increase of the individual bond angles Ru(Cr)–O-Ru(Cr) and the average bond angle $\langle$Ru(Cr)–O-Ru(Cr)$\rangle$, and the structure evolves toward the undistorted cubic aristotype [Fig. 7(c)]. One may wonder if observed increase of T_c with Cr substitution is related to a smaller deviation of the $\langle$Ru(Cr)–O-Ru(Cr)$\rangle$ bond angle from 180°.[2,4,11] That this cannot be the case is evident from the fact that under pressure T_c is found to decrease[5] and from observation of a nonmonotonic change of T_c with increase of the $\langle$Ru(Cr)–O-Ru(Cr)$\rangle$ bond angle [Fig. 7(c) and Fig. 4].

To establish the formal valence of the Ru and Cr ions for substituted samples we have measured the average Ru(Cr)–O bond lengths [Fig. 7(d)]. Using Shannon data[18] for ionic sizes of the six-coordinated Ru^{4+}, Ru^{5+}, Cr^{3+}, and Cr^{4+}, and by taking the oxygen ionic size of 1.365 Å to match the measured average $\langle$Ru(Cr)–O$\rangle$ bond length in $SrRuO_3$ with the calculated sum of the ionic sizes of $R(Ru^{4+})+R(O^{2-})$ from Shannon tables, we have obtained the two lines shown on Fig. 7(d). The average measured $\langle$Ru(Cr)–O$\rangle$ bond lengths are shorter than predicted by formation of either Ru^{5+} and Cr^{3+} or Ru^{4+} and Cr^{4+}, but are closer to the Ru^{4+} and Cr^{4+} line. This is consistent with the charge balance of the $Sr(Ru^{4+}{}_{1-x}Cr^{4+}{}_x)O_3$ configuration in agreement with results of measurements of the effective paramagnetic moment. This again indicates the presence of Cr^{4+} ions and supports a model of double exchange interactions between the minority Ru t_{2g} band and the Cr t_{2g} band.

Numerous structural studies of perovskites supported by group-theoretical analysis[19] have shown that the temperature or composition induced transformation of the orthorhombic *Pbnm* structure to the cubic undistorted *Pm3m* structure involves intermediate pseudotetragonal *Imma* and tetragonal $I4/mcm$ structures. In our study, however, we did not reach the region of the *Imma* phase. The inset of Fig. 6 illustrates the presence of the reflections forbidden in *Imma* by its higher symmetry for the sample with the highest studied substitution, $x=0.20$, and the refinement of diffraction data for this sample using *Imma* model resulted in significantly worse agreement factors R_p, R_{wp}, and χ^2 equal 5.01%, 7.46%, and 2.73 vs 3.33%, 5.16%, and 1.31 for *Pbnm*, respectively.

On the other hand, using the approach of calculating the tolerance factor $t(x)$ as a function of composition from the average interatomic distances $\langle$Sr–O$\rangle$ and $\langle Ru_{1-x}Cr_x-O\rangle$ of the perovskite A- and B-site cations, respectively,[20] we can predict the lower limit of the stability range of $Sr(Ru_{1-x}Cr_x)O_3$ in a cubic perovskite structure. The tolerance factor $t(x)=(A-O)/\sqrt{2}(B-O)$ increases linearly with Cr content, x, reflecting the linear decrease of the average ionic radius of the B-site cation [Fig. 7(e)]. From extrapolation of the tolerance factor to unity we expect the unit cell metrics to become cubic at room temperature when $x_{\text{cubic}}\sim 0.51$. Since the tolerance factor is an increasing function of temperature,[20] we expect to approach the cubic phase ($t=1$) for lower substitution levels at elevated temperatures. Indeed, the observed solubility limit at $x\sim 0.15$ is a result of exceeding the condition of stability of the perovskite phase, $t\leqslant 1$, at the synthesis temperature of ~1300 °C. By using reduced oxygen pressure synthetic schemes we have been able to extend the composition range over which the perovskite phase can be formed for several mixed-valent transition metals that can accommodate variable coordination to oxygen.[21–24] However, this method of extending the solubility limit has not been successful for substitution of Cr for Ru due to their fixed coordination number with oxygen. Thus,

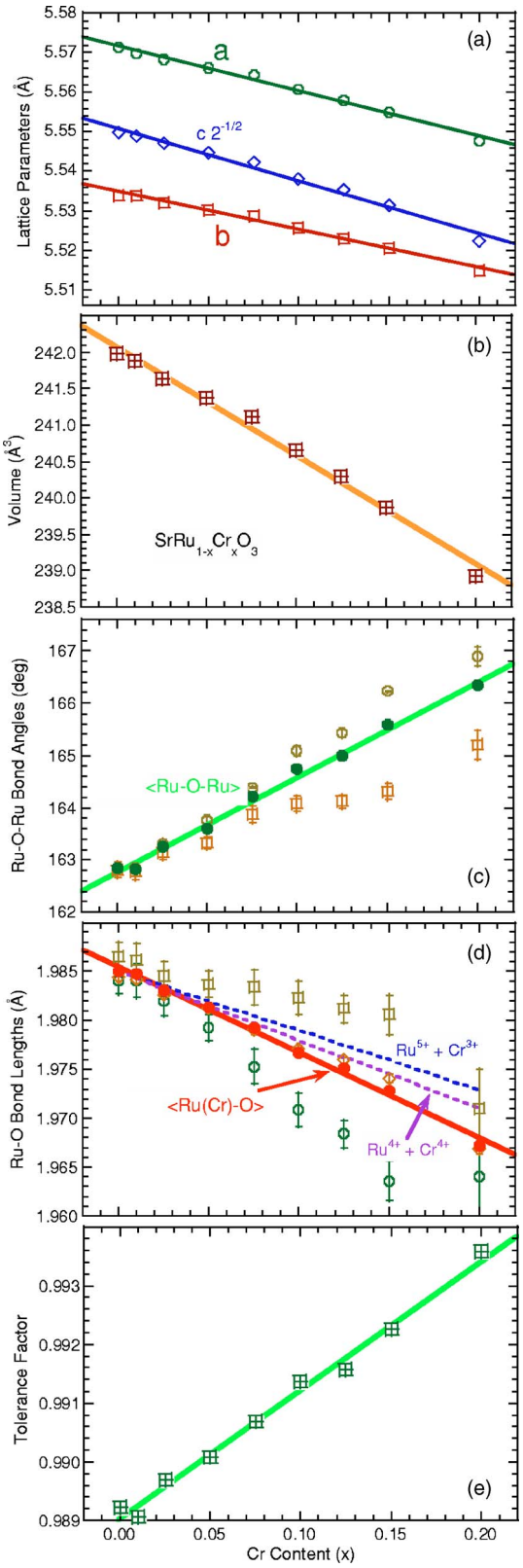

FIG. 7. (Color online) (a) Cell parameters, (b) cell volume, (c) bond angles Ru(Cr)-O-Ru(Cr), (d) bond lengths Ru(Cr)-O, and (e) tolerance factor as a function of composition for $Sr(Ru_{1-x}Cr_x)O_3$ at room temperature. Lines are linear fits to the data.

we were not able to decrease the tolerance factor during the synthesis by the introduction of oxygen vacancies that would reduce the valence of Ru and Cr, effectively increasing their ionic sizes. The only favorable method found so far to increase the solubility is synthesis under high temperature and high-pressure conditions. An application of the high hydrostatic pressure decreases the ionic *A*-O bonds stronger than the covalent *B*-O bonds causing reduction of the tolerance factor and this leads to the extension of the solubility range. We will use the method of synthesis at very high pressures in future studies of the $SrRu_{1-x}Cr_xO_3$ system with compositions $x > 0.20$.

IV. CONCLUSIONS

We have studied the structural, magnetic, and resistive properties of the $SrRu_{1-x}Cr_xO_3$ perovskites with uniquely increased ferromagnetic transition temperatures from 163 to 188 K. Polycrystalline samples synthesized in air at 1340 °C reach the Cr solubility limit at $x=0.15$. This substitution limit was increased using high-pressure high-temperature synthetic techniques. The limited chromium substitution is controlled by geometrical constraints of the tolerance factor and is consistent with a linear decrease of the lattice parameters and bond lengths, and an increase of the bond angles with increasing x due to substitution of the smaller $Cr^{4+/3+}$ ion for $Ru^{4+/5+}$. Similar decreases of the molar susceptibility, χ_m, in the paramagnetic region above T_c and the high-field magnetization at 5 K with x also indicate the presence of the $Cr^{4+/3+}$ and $Ru^{4+/5+}$ ions. These results are in agreement with NMR studies[14] and confirm that the $Ru^{4+/5+}(d^{4/3})$-O^{2-}-$Cr^{4+/3+}(d^{2/3})$ minority band double-exchange interaction which involves the Cr^{3+} and Cr^{4+} in the magnetic ordering is responsible for the enhanced ordering temperature. The reduced coercive fields determined from the magnetization curves and a minimum of resistivity point to decreased disorder for slightly substituted compositions of $x \sim 0.025$.

Results presented here indicate that through simple chemical substitution one could prevent the formation of Ru vacancies while simultaneously enhancing the electronic and magnetic properties of $SrRuO_3$. Similar enhancements of useful properties by creative substitutions and extension of achievable compositions have been used previously to control the properties of manganites.[21–24] These methods can be extended to other transition metal perovskites and other oxides.

ACKNOWLEDGMENTS

We wish to thank Simine Short for her technical support. Work at NIU was supported by the NSF-DMR-0302617. At ANL, work was supported by the U.S. Department of Energy, Office of Science under Contract No. W-31-109-ENG-38.

[1] L. Klein, J. S. Dodge, C. H. Ahn, J. W. Reiner, L. Mieville, T. H. Geballe, M. R. Beasley, and A. Kapitulnik, J. Phys.: Condens. Matter **8**, 10111 (1996).
[2] I. I. Mazin, and D. J. Singh, Phys. Rev. B **56**, 2556 (1997).
[3] C. B. Eom, R. J. Cava, R. M. Fleming, Julia M. Phillips, R. B. van Dover, J. H. Marshall, J. W. P. Hsu, J. J. Krajewski, and W. F. Peck, Jr., Science **258**, 1766 (1992).
[4] G. Cao, S. McCall, M. Shepard, J. E. Crow, and R. P. Guertin, Phys. Rev. B **56**, 321 (1997).
[5] J. J. Neumeier, A. L. Cornelius, and J. S. Schilling, Physica B **198**, 324 (1994).
[6] B. Dabrowski, O. Chmaissem, P. W. Klamut, S. Kolesnik, M. Maxwell, J. Mais, Y. Ito, and B. D. Armstrong, Phys. Rev. B **70**, 014423 (2004).
[7] B. Dabrowski, O. Chmaissem, S. Kolesnik, P. W. Klamut, M. Maxwell, M. Avdeev, and J. D. Jorgensen, Phys. Rev. B **71**, 104411 (2005).
[8] Q. Gan, R. A. Rao, C. B. Eom, J. L. Garrett, and M. Lee, Appl. Phys. Lett. **72**, 978 (1998).
[9] G. Cao, F. Freibert, and J. E. Crow, J. Appl. Phys. **81**, 3884 (1997).
[10] T. He and R. J. Cava, Phys. Rev. B **63**, 172403 (2001).
[11] A. Kanbayasi, J. Phys. Soc. Jpn. **44**, 108 (1978).
[12] M. Shepard, G. Cao, S. McCall, F. Freibert, and J. E. Crow, J. Appl. Phys. **79**, 4821 (1996).
[13] L. Pi, A. Maignan, R. Retoux, and B. Raveau, J. Phys.: Condens. Matter **14**, 7391 (2002).
[14] Z. H. Han, J. I. Budnick, W. A. Hines, B. Dabrowski, S. Kolesnik, and T. Maxwell, J. Phys.: Condens. Matter **17**, 1193 (2005).
[15] J. D. Jorgensen, J. Faber, Jr., J. M. Carpenter, R. K. Crawford, J. R. Haumann, R. L. Hittermann, R. Kleb, G. E. Ostrowski, F. J. Rotella, and T. G. Worlton, J. Appl. Crystallogr. **22**, 321 (1989).
[16] A. C. Larson and R. B. Von Dreele, Los Alamos Natl. Lab., LAUR 86-748, 1994.
[17] B. H. Toby, J. Appl. Crystallogr. **34**, 210 (2001).
[18] R. D. Shannon, Acta Crystallogr., Sect. A: Cryst. Phys., Diffr., Theor. Gen. Crystallogr. **A32**, 751 (1976).
[19] C. J. Howard and H. T. Stokes, Acta Crystallogr., Sect. A: Found. Crystallogr. **A61**, 93 (2004) and references therein.
[20] B. Dabrowski, O. Chmaissem, J. Mais, S. Kolesnik, J. D. Jorgensen, and S. Short, J. Solid State Chem. **170**, 154 (2003).
[21] O. Chmaissem, B. Dabrowski, S. Kolesnik, J. Mais, D. E. Brown, R. Kruk, P. Prior, B. Pyles, and J. D. Jorgensen, Phys. Rev. B **64**, 134412 (2001).
[22] O. Chmaissem, B. Dabrowski, S. Kolesnik, J. Mais, J. D. Jorgensen, and S. Short, Phys. Rev. B **67**, 094431 (2003).
[23] S. Kolesnik, B. Dabrowski, J. Mais, D. E. Brown, R. Feng, O. Chmaissem, R. Kruk, and C. W. Kimball, Phys. Rev. B **67**, 144402 (2003).
[24] E. N. Caspi, M. Avdeev, S. Short, J. D. Jorgensen, B. Dabrowski, O. Chmaissem, J. Mais, and S. Kolesnik, J. Solid State Chem. **177**, 1456 (2004).